Mon. Not. R. Astron. Soc. **349,** 1039–1051 (2004) doi:10.1111/j.1365-2966.2004.07586.x

The inner structure of ΛCDM haloes – III. Universality and asymptotic slopes

J. F. Navarro,[1★†] E. Hayashi,[1] C. Power,[2] A. R. Jenkins,[2] C. S. Frenk,[2] S. D. M. White,[3] V. Springel,[3] J. Stadel[4] and T. R. Quinn[5]

[1]*Department of Physics and Astronomy, University of Victoria, Victoria, BC, V8P 1A1, Canada*
[2]*Institute for Computational Cosmology, Department of Physics, University of Durham, South Road, Durham DH1 3LE*
[3]*Max-Planck Institute for Astrophysics, Garching, Munich, D-85740, Germany*
[4]*Institute for Theoretical Physics, University of Zurich, Zurich CH-8057, Switzerland*
[5]*Department of Astronomy, University of Washington, Seattle, WA 98195, USA*

Accepted 2003 December 29. Received 2003 December 20; in original form 2003 November 11

ABSTRACT

We investigate the mass profile of cold dark matter (ΛCDM) haloes using a suite of numerical simulations spanning five decades in halo mass, from dwarf galaxies to rich galaxy clusters. These haloes typically have a few million particles within the virial radius (r_{200}), allowing robust mass profile estimates down to radii <1 per cent of r_{200}. Our analysis confirms the proposal of Navarro, Frenk & White (NFW) that the shape of the ΛCDM halo mass profiles differs strongly from a power law and depends little on mass. The logarithmic slope of the spherically averaged density profile, as measured by $\beta = -\mathrm{d}\ln\rho/\mathrm{d}\ln r$, decreases monotonically towards the centre and becomes shallower than isothermal ($\beta < 2$) inside a characteristic radius, r_{-2}. The fitting formula proposed by NFW provides a reasonably good approximation to the density and circular velocity profiles of individual haloes; circular velocities typically deviate from NFW best fits by <10 per cent over the radial range that is numerically well resolved. Alternatively, systematic deviations from the NFW best fits are also noticeable. Inside r_{-2}, the profile of simulated haloes becomes shallower with radius more gradually than predicted and, as a result, NFW fits tend to underestimate the dark matter density in these regions. This discrepancy has been interpreted as indicating a steeply divergent cusp with asymptotic inner slope, $\beta_0 \equiv \beta(r = 0) \sim 1.5$. Our results suggest a different interpretation. We use the density and enclosed mass at our innermost resolved radii to place strong constraints on β_0: density cusps as steep as $r^{-1.5}$ are inconsistent with most of our simulations, although $\beta_0 = 1$ is still consistent with our data. Our density profiles show no sign of converging to a well-defined asymptotic inner power law. We propose a simple formula that reproduces the radial dependence of the slope better than the NFW profile, and so may minimize errors when extrapolating our results inward to radii not yet reliably probed by numerical simulations.

Key words: gravitation – cosmology: theory – dark matter.

1 INTRODUCTION

Disc galaxy rotation curves; strong gravitational lensing by galaxies and clusters; the dynamics of stars in elliptical galaxies and of gas and galaxies in clusters; these are just examples of the various luminous tracers that probe the inner structure of dark matter haloes. Such observations place strong constraints on the distribution of dark matter in these highly non-linear regions that may be contrasted directly with theoretical predictions for halo structure. Given the sensitivity of such predictions to the nature of the dark matter, these observational constraints constitute provide tests that may question or even rule out particular models of dark matter.

Robust prediction of the inner structure of cold dark matter (CDM) haloes is a quintessential N-body problem, albeit one of considerable complexity due to the large overdensities and, consequently, the short crossing times involved. Indeed, only recently have computational capabilities improved to the point of allowing realistic simulation of the regions which house the luminous components of individual galaxies.

★Fellow of the Canadian Institute for Advanced Research and of the J.S. Guggenheim Memorial Foundation.
†E-mail: jfn@uvic.ca

This work builds upon the pioneering efforts of Frenk et al. (1988), Dubinski & Carlberg (1991) and Crone, Evrard & Richstone (1994), among others, which led to the identification of a number of key features of the structure of dark matter haloes assembled by hierarchical clustering. One important result of this early work concerns the absence of a well-defined central 'core' of constant density in virialized CDM haloes. In this sense, dark matter haloes are 'cuspy': the dark matter density increases apparently without bounds towards the centre of the halo.

A second result concerns the remarkable similarity ('universality') in the structure of dark matter haloes of widely different mass. This was first proposed by Navarro, Frenk & White (1996, 1997, hereafter NFW), who suggested a simple fitting formula to describe the spherically averaged density profiles of dark matter haloes:

$$\rho(r) = \frac{\rho_{\rm s}}{(r/r_{\rm s})[1+(r/r_{\rm s})]^2}, \tag{1}$$

where $\rho_{\rm s}$ and $r_{\rm s}$ are the characteristic density and radius, respectively. The larger the mass of a halo, the lower its characteristic density, reflecting the lower density of the universe at the (later) assembly time of more massive systems.

Further simulation work of similar numerical resolution (see, e.g. Cole & Lacey 1996; Huss, Jain & Steinmetz 1999) provided support for the NFW conclusions, although small but systematic differences began to emerge as the numerical resolution of the simulations improved (see, e.g. Moore et al. 1999, hereafter M99, Ghigna et al. 2000; Fukushige & Makino 1997, 2001, 2003). These authors reported deviations from equation (1) that increase systematically inwards, and thus are particularly noticeable in high-resolution simulations. In particular, Fukushige & Makino (2001) reported that NFW fits tend to underestimate the dark matter density within the scale radius $r_{\rm s}$. M99 reached a similar conclusion and interpreted this result as indicating a density cusp steeper than that of the NFW profile. These authors preferred a modified fitting function which diverges as $r^{-1.5}$ near the centre:

$$\rho(r) = \frac{\rho_{\rm M}}{(r/r_{\rm M})^{1.5}\left[1+(r/r_{\rm M})^{1.5}\right]}. \tag{2}$$

One should note, however, that there is no consensus amongst N-body practitioners for such a modified profile (see, e.g. Klypin et al. 2001; Power et al. 2003, hereafter P03), and that there is some work in the literature suggesting that the central density cusp might actually be *shallower* than r^{-1} (Subramanian, Cen & Ostriker 2000; Taylor & Navarro 2001; Ricotti 2003).

This unsettled state of affairs illustrates the difficulties associated with simulating the innermost structure of CDM haloes in a reliable and reproducible manner. The high density of dark matter in such regions demands large numbers of particles and fine time resolution, pushing to the limit even the largest supercomputers available at present. As a result, many of the studies mentioned above either are of inadequate resolution to be conclusive or are based on results from a handful of simulations where computational cost precludes a systematic assessment of numerical convergence.

Establishing the detailed properties of the central density cusp, as well as deriving the value of its asymptotic central slope, is important for a number of reasons. For example, steeper cusps place larger amounts of dark matter at the centre, exacerbating the disagreement with observations that suggest the presence of a constant-density core in low surface brightness galaxies or in strongly barred galaxies (Moore 1994; Flores & Primack 1994; McGaugh & de Blok 1998; Debattista & Sellwood 1998; van den Bosch et al. 2000). Steep cusps would also be important for direct detection experiments for dark matter, as a possible gamma-ray annihilation signal of weakly interacting massive particles (WIMPS) at the Galactic Centre would be particularly strong for $r^{-1.5}$ cusps (Calcáneo-Roldán & Moore 2000; Stoehr et al. 2002; Taylor & Silk 2003).

Finally, the detailed structure of the central cusp is not the only focus of contrasting claims in the literature. For example, the 'universality' of the CDM halo structure has been questioned by Jing & Suto (2000), who find that the slope of the density profile at a fixed fraction of the virial radius steepens towards lower halo masses. Klypin et al. (2001), alternatively, point out that such a systematic trend is entirely consistent with universality as originally claimed by NFW, and just reflects the mass dependence of halo characteristic density.

We address these conflicting issues here using a suite of 19 high-resolution simulations of the formation of haloes in the standard ΛCDM cosmogony. Halo masses are chosen in three main groups: 'dwarf' haloes with $M_{200} \sim 10^{10}\ h^{-1}\ {\rm M}_\odot$, 'galaxy' haloes with $M_{200} \sim 10^{12}\ h^{-1}\ {\rm M}_\odot$ and 'cluster' haloes of mass $M_{200} \sim 10^{15}\ h^{-1}\ {\rm M}_\odot$. This allows us to gain insight into the effects of cosmic variance at each mass scale, as well as to explore the mass dependence of the structure of ΛCDM haloes. We define the mass of a halo to be that contained within its virial radius, that is, within a sphere of mean density contrast 200.[1]

This paper is organized as follows. Section 2 describes briefly the numerical simulations; Section 3 discusses our main results; and we summarize our conclusions in Section 4.

2 NUMERICAL EXPERIMENTS

The numerical set up of our simulations follows closely the procedure described by P03, where the interested reader may find a thorough discussion of our initial conditions generating scheme, the choice of N-body codes and integrators, as well as the criteria adopted to optimize the choice of the numerical parameters of the simulations. For completeness, we include here a brief discussion of the main numerical issues, but refer the reader to P03 for a more detailed discussion.

2.1 *N*-body codes

The simulations reported in this paper have been performed using two parallel N-body codes: GADGET, written by Volker Springel (Springel, Yoshida & White 2001), and PKDGRAV, written by Joachim Stadel and Thomas Quinn (Stadel 2001). As discussed in P03, both codes give approximately the same results for appropriate choices of numerical parameters, and neither code seems obviously to outperform the other when similar numerical convergence criteria are met.

2.2 Cosmological model

We adopt a flat, $\Omega_0 = 0.3$ ΛCDM cosmological model the dynamics of which is dominated at present by a cosmological constant, $\Omega_\Lambda = 0.7$. The matter power spectrum is normalized so that the present linear rms amplitude of mass fluctuations in spheres of radius $8\ h^{-1}$ Mpc is $\sigma_8 = 0.9$. We assume a linear fluctuation power spectrum

[1] We use the term 'density contrast' to denote densities expressed in units of the critical density for closure, $\rho_{\rm crit} = 3H^2/8\pi G$. We express the present value of Hubble's constant as $H(z=0) = H_0 = 100\ h$ km s^{-1} Mpc^{-1}.

Table 1. The parameters of the parent cosmological simulations.

Label	$L_{\rm box}$ (h^{-1} Mpc)	$z_{\rm i}$	$m_{\rm p}$ (h^{-1} M$_\odot$)	ϵ (h^{-1} kpc)	Code
ENS01	32.5	49.0	1.36×10^9	10	AP3M
SGIF-128	35.325	49.0	1.75×10^9	10	GADGET
ΛCDM-512	479.0	36.0	6.82×10^{10}	30	GADGET

given by the product of the square of the appropriate CDM transfer function, $T^2(k)$, and a Harrison–Zel'dovich primordial power spectrum [i.e. $P(k) \propto k$].

2.3 Parent simulations

The halo samples were drawn from three different ΛCDM cosmological 'parent' simulations. Table 1 lists the main numerical parameters of each of these simulations: $L_{\rm box}$ is the size of the cosmological box, $z_{\rm i}$ is the initial redshift, $m_{\rm p}$ is the particle mass, and ϵ is the softening parameter; assumed to be fixed in comoving coordinates.

The dwarf, cluster and most of the galaxy haloes were extracted from the ΛCDM-512 (Yoshida, Sheth & Diaferio 2001) and SGIF-128 simulations. These two parent simulations, both carried out within the Virgo Consortium, used the CDM transfer function given by CMBFAST (Seljak & Zaldarriaga 1996), assuming $h = 0.7$ and $\Omega_{\rm b} = 0.04$. This transfer function is well fitted by the Bardeen et al. (1986) fitting formula with a value of 0.17 for the shape parameter Γ. Three of the galaxy haloes (G1–G3, see Table 2) were extracted from the parent simulation described by (labelled ENS01 in Table 1 Eke, Navarro & Steinmetz (2001, labelled ENS01 in Table 1). That simulation used the Bardeen et al. (1986) fitting formula for the CDM transfer function, with $h = 0.65$ and $\Gamma = 0.2$.

2.4 Initial conditions

Since completing the numerical convergence tests reported in P03, we have developed a more flexible and powerful set of codes for setting up the resimulation initial conditions. This resimulation software enables us to iterate the procedure to 'resimulate a resimulation', an important step for setting up appropriate initial conditions for dwarf haloes. The basic methodology employed is very similar to the methods described in P03, with just a few minor differences. Galaxy haloes G1–G3 were selected from the ENS01 simulation and their initial conditions were created using the software described in P03. All of the other haloes were set up with the new codes, following the procedure we describe below.

The first stage is to carry out, up to the redshift of interest (typically $z = 0$), a 'parent' simulation of a large, representative volume of a ΛCDM universe. These parent simulations are used to select haloes targeted for resimulation at higher resolution. Once a halo has been selected for resimulation at $z = 0$, we trace all particles within a sphere of radius $\sim 3r_{200}$ to the $z = \infty$ 'unperturbed' configuration. We then create a set of initial conditions with much higher mass resolution in the volume occupied by the halo particles, and resample the remainder of the periodic box at lower resolution, taking care to retain sufficient resolution in the regions surrounding the halo of interest so that external tidal forces acting on the high-resolution region are adequately represented.

The procedure involves two main steps. First, we set up a uniform multi-mass distribution of particles to approximate the particle positions in the high-resolution region at $z = \infty$. This is accomplished by arranging particles either in a cubic grid or as a 'glass', within a cube just big enough to contain the region of interest. Either choice approximates a uniform mass distribution very accurately. Outside the cube we lay down particles on a set of concentric cubic shells, centred on the cube, which extend outwards until they fill the entire periodic volume of the parent simulation. These concentric shells are filled with more massive particles whose interparticle separation increases approximately linearly with distance from the high-resolution region. Unlike the grid or glass, this arrangement does not reproduce a perfectly uniform mass distribution. However, by populating each shell with regularly spaced particles, we obtain a configuration which is uniform enough for our purposes.

In the interest of efficiency, we replace those particles in the high-resolution cube that do not end up in the selected halo with more massive particles made by combining several high-resolution ones. This procedure, particularly for the dwarf halo resimulations,

Table 2. The main parameters of the resimulated haloes.

Label	$z_{\rm i}$	ϵ (h^{-1} kpc)	N_{200}	M_{200} (h^{-1} M$_\odot$)	r_{200} (h^{-1} kpc)	V_{200} (km s^{-1})	$r_{\rm conv}$ (h^{-1} kpc)	Code
D1	74	0.0625	784980	7.81×10^9	32.3	32.3	0.34	GADGET
D2	49	0.0625	778097	9.21×10^9	34.1	34.1	0.37	GADGET
D3	49	0.0625	946421	7.86×10^9	32.3	32.3	0.33	GADGET
D4	49	0.0625	1002098	9.72×10^9	34.7	34.7	0.32	GADGET
G1	49	0.15625	3447447	2.29×10^{12}	214.4	214.4	1.42	GADGET
G2	49	0.5	4523986	2.93×10^{12}	232.6	232.6	1.25	PKDGRAV
G3	49	0.45	2661091	2.24×10^{12}	212.7	212.7	1.65	PKDGRAV
G4	49	0.3	3456221	1.03×10^{12}	164.0	164.0	1.01	PKDGRAV
G5	49	0.35	3913956	1.05×10^{12}	165.0	165.0	1.02	PKDGRAV
G6	49	0.35	3739913	9.99×10^{11}	162.5	162.5	1.03	PKDGRAV
G7	49	0.35	3585676	9.58×10^{11}	160.3	160.3	1.02	PKDGRAV
C1	36	5.0	1565576	7.88×10^{14}	1502.1	1502.1	16.8	GADGET
C2	36	5.0	1461017	7.36×10^{14}	1468.1	1468.1	16.9	GADGET
C3	36	5.0	1011918	5.12×10^{14}	1300.6	1300.6	16.1	GADGET
C4	36	5.0	1050402	5.31×10^{14}	1316.7	1316.7	15.9	GADGET
C5	36	5.0	1199299	6.05×10^{14}	1375.5	1375.5	16.2	GADGET
C6	36	5.0	1626161	8.19×10^{14}	1521.1	1521.1	15.5	GADGET
C7	36	5.0	887837	4.50×10^{14}	1245.8	1245.8	16.4	GADGET
C8	36	5.0	1172850	5.92×10^{14}	1365.4	1365.4	16.8	GADGET

significantly reduces the number of particles in the initial conditions and the run time of the subsequent simulation. Thus, each halo forms from an 'amoeba-shaped' region consisting only of the highest resolution particles in the hierarchy. We have explicitly checked that the resampling procedure adds no extra power; in tests, the multi-mass particle distribution remains very close to uniform over an expansion factor of up to ∼50.

Once a multi-mass but uniform mass distribution has been created, the next step is to add the appropriate Gaussian density fluctuations. This is done by assigning a displacement and a peculiar velocity to each particle using Fourier methods. By using the same amplitude and phase for every Fourier mode present in the parent simulation, a perturbed density field essentially identical to that of the parent simulation can be reproduced. In the high-resolution cube, because the particle mass is smaller than in the parent simulation, it is necessary to add additional short-wavelength modes (with amplitudes fixed by the adopted power spectrum) down to the Nyquist wavelength of the new particle grid. To ensure that the Fourier transforms needed to add this extra power are of a manageable size, we make the additional power periodic on the scale of the central cube rather than on the scale of the parent simulation. The longest wavelength added is typically smaller than one tenth of the side length of the original cube. As described in P03, the individual components of the displacement field are generated in turn, and the displacements calculated at the particle positions by trilinear interpolation. To set up growing modes, we use the Zel'dovich approximation and make the peculiar velocities proportional to the displacements.

The initial redshift, z_i, of each resimulation is chosen so that density fluctuations in the high-resolution region are in the linear regime. P03 find that convergent results are obtained when z_i is high enough that the (theoretical) rms mass fluctuation on the smallest resolved mass scale, $\sigma(m_p, z_i)$ does not exceed ∼0.3 (where m_p is the mass of a high-resolution particle). All of our simulations satisfy this criterion.

2.5 Halo selection

The resimulated haloes analysed in this paper were all identified in the parent simulations by applying the friends-of-friends (FoF) group-finding algorithm (Davis et al. 1985) with a linking length $l = 0.164$. Cluster-sized haloes were drawn from a 479 h^{-1} Mpc simulation volume (ΛCDM-512 in Table 1). The FoF(0.164) groups were first ordered by mass and then 10 consecutive entries on the list centred around a mass of $10^{15}h^{-1}$ $M_\odot$ were selected. Galaxy haloes were likewise drawn from a 35.325 h^{-1} Mpc volume (SGIF-128), with the exception of three of the haloes (G1–G3) which were selected from a 32.5 h^{-1} Mpc volume (ENS01).

Target dwarf haloes were also found in the SGIF-128 simulation. However, owing to their extremely low mass (corresponding to five to six particles in SGIF-128), it was necessary to create a second 'parent' simulation for them by resimulating a region of the SGIF-128 volume at significantly higher resolution. To this end, a spherical region of radius 4.4 h^{-1} Mpc, with mean density close to the universal average, was selected at random within the 35.325 h^{-1} Mpc box. This spherical region was then resimulated with roughly 100 times more particles than in SGIF-128. The target dwarf haloes were identified within this spherical volume again from an FoF(0.2) group list. A total of 18 haloes with 450–550 particles (corresponding to masses of 9–11 × 10^9h^{-1} $M_\odot$) were chosen. We report results on the four haloes in this list that have been resimulated to date. High-resolution initial conditions for these dwarf haloes were created in an identical way to the more massive galaxy and cluster haloes.

Numerical parameters were chosen to ensure that all haloes, regardless of mass, were resimulated at a comparable mass resolution (typically over 10^6 particles within the virial radius at $z = 0$, see Table 2).

2.6 The analysis

We focus our analysis on the spherically averaged mass profile of simulated haloes at $z = 0$. This is measured by sorting particles in distance from the centre of each halo and arranging them in bins of equal logarithmic width in radius. Density profiles, $\rho(r)$, are computed simply by dividing the mass in each bin by its volume. The cumulative mass within each bin, $M(r)$, is then used to compute the circular velocity profile of each halo, $V_c(r) = \sqrt{GM(r)/r}$, as well as the cumulative density profile, $\bar{\rho}(r) = 3M(r)/4\pi r^3$, which we shall use in our analysis.

The centre of each halo is determined using an iterative technique in which the centre of mass of particles within a shrinking sphere is computed recursively until a few thousand particles are left (see P03 for details). In a multi-component system, such as a dark halo with substructure, this centring procedure isolates the densest region within the largest subcomponent. In more regular systems, the centre so obtained approximately coincides with the centres defined by the centre of mass weighted by the local density or by the gravitational potential of each particle.

We note that, unlike in NFW, no attempt has been made to select haloes at a particularly quiet stage in their dynamical evolution; our sample thus contains haloes in equilibrium as well as a few with prominent substructures as a result of recent accretion events.

2.7 Parameter selection criteria

The analysis presented in P03 demonstrated that the mass profile of a simulated halo is numerically robust down to a 'convergence radius', r_{conv}, that depends primarily on the number of particles and time-steps, as well as on the choice of gravitational softening in the simulation. Each of these choices imposes a minimum radius for convergence, although for an 'optimal' choice of parameters (i.e. one that, for given r_{conv}, minimizes the number of force computations and time-steps) the most stringent criterion is that imposed by the number of particles within r_{200}. In this optimal case, the minimum resolved radius is well approximated by the location at which the two-body relaxation time, t_{relax}, equals the age of the universe [see Hayashi et al. (2004) for further validation of these criteria, but see Binney (2004) for a different opinion].

To be precise, we shall identify r_{conv} with the radius where t_{relax} equals the circular orbital time-scale at the virial radius, $t_{circ}(r_{200}) = 2\pi\, r_{200}/V_{200}$. Thus, r_{conv} is defined by the following equation:

$$\frac{t_{relax}(r)}{t_{circ}(r_{200})} = \frac{N}{8\ln N}\frac{r/V_c}{r_{200}/V_{200}} = 1. \quad (3)$$

Here $N = N(r)$ is the number of particles enclosed within r and $V_{200} = V_c(r_{200})$. With this definition, the convergence radius in our best-resolved haloes, outside which $V_c(r)$ converges to better than 10 per cent, is of order $\sim 0.005 r_{200}$.

3 RESULTS

3.1 Density profiles

The top panels of Fig. 1 show the density profiles, $\rho(r)$, of the 19 simulated haloes in our sample. In physical units, the profiles

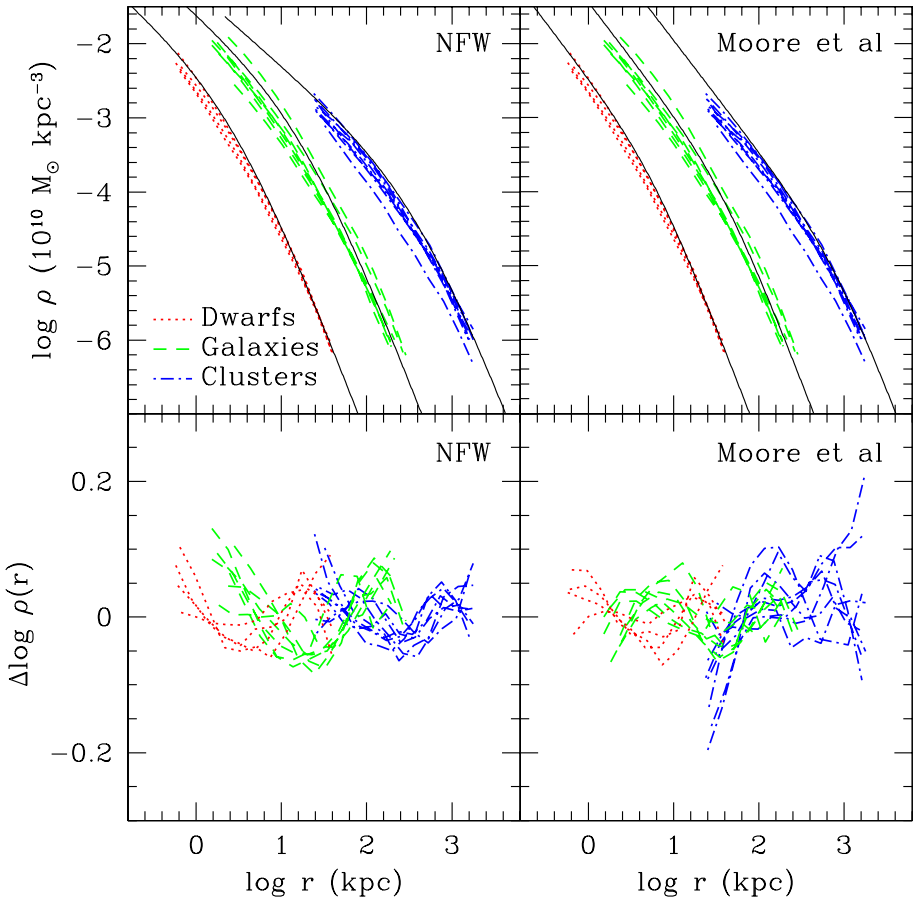

Figure 1. Spherically averaged density profiles of all our simulated haloes. Densities are computed in radial bins of equal logarithmic width and are shown from the innermost converged radius ($r_{\rm conv}$) out to about the virial radius of each halo (r_{200}). Our simulations target haloes in three distinct mass groups: 'dwarf', 'galaxy' and 'cluster' haloes. These groups span more than five decades in mass. Thick solid lines in the top panels illustrate the expected halo profile for each mass range according to the fitting formula proposed by NFW (top left) or M99 (top right). The bottom panels indicate the deviation from the *best* fit achieved for each individual halo (simulation minus fit) with the NFW profile (equation 1) or with its modified form, as proposed by M99 (equation 2).

split naturally into three groups: from left to right, 'dwarf' (dotted), 'galaxy' (dashed) and 'cluster' (dot-dashed) haloes, respectively. Each profile is shown from the virial radius, r_{200}, down to the innermost converged radius, $r_{\rm conv}$; a convention that we shall adopt in all figures throughout this paper.

The thick solid lines in the top-left panel show the NFW profiles (equation 1) expected for haloes in each group, with parameters chosen according to the prescription of Eke et al. (2001). Note that these NFW curves are *not* best fits to any of the simulations, but that they still capture reasonably well the shape and normalization of the density profiles of the simulated haloes.

The top-right panel of Fig. 1 is similar to the top-left one, but the comparison is made here with the modified form of the NFW profile proposed by M99 (equation 2). There is no published prescription specifying how to compute the numerical parameters of this formula for haloes of given mass, so the three profiles shown in this panel are just 'eyeball' fits to one halo in each group. Like the NFW profile, the M99 formula also appears to describe reasonably well the gently curving density profiles of ΛCDM haloes.

Fig. 1 thus confirms a number of important trends that were already evident in prior simulation work.

(i) ΛCDM halo density profiles deviate significantly from simple power laws, and steepen systematically from the centre outwards; they are shallower than isothermal near the centre and steeper than isothermal near the virial radius.

(ii) There is no indication of a well-defined central 'core' of constant density; the dark matter density keeps increasing all the way in, down to the innermost resolved radius.

(iii) Simple formulae such as the NFW profile (equation 1) or the M99 formula (equation 2) appear to describe the mass profile of all haloes reasonably well, irrespective of mass, signalling a 'universal' profile shape. Properly scaled, a dwarf galaxy halo is almost indistinguishable from a galaxy cluster halo.

We elaborate further on each of these conclusions in the following subsections.

3.1.1 *NFW versus M99 fits*

Are the density profiles of ΛCDM haloes described better by the NFW formula (equation 1) or by the modification proposed by M99 (equation 2)? The answer may be seen in the bottom panels of Fig. 1. These panels show the deviations (simulation minus fit) from the *best* fits to the density profiles of each halo using the NFW profile or the M99 profile. These fits are obtained by straightforward χ^2 minimization, assigning equal weight to each radial bin. This is done because the statistical (Poisson) uncertainty in the determination of

the density within each bin is negligible (each bin contains several thousand to several hundred thousand particles) so the remaining uncertainties are likely to be dominated by systematics, such as the presence of substructure, varying asphericity, as well as numerical error, whose radial dependence is difficult to assess quantitatively (see P03).

As shown in the bottom panels of Fig. 1, there is significant variation in the shape of the density profile from one halo to another. Some systems are fitted better by equation (1) than by equation (2), and the reverse is true in other cases. Over the radial range resolved by the simulations, $\rho(r)$ deviates from the best fits by less than ∼50 per cent. NFW fits tend to *underestimate* the density in the inner regions of most haloes: by up to 35 per cent at the innermost resolved point. M99 fits, on the other hand, seem to do better for low-mass haloes, but tend to *overestimate* the density in the inner regions of cluster haloes by up to 60 per cent. We have explicitly checked that these conclusions are robust to reasonable variation in the binning used to construct the density profiles, as well as in the adopted minimization procedure.

This level of accuracy may suffice for a number of observational applications, with the proviso that comparisons are restricted to radii where numerical simulations are reliable; i.e. $r_{\rm conv} < r < r_{200}$. Deviations from the best fits increase systematically towards the centre, so it is likely that extrapolations of either fitting formula to radii much smaller than $r_{\rm conv}$ will incur substantial error. We discuss below (Section 3.6) possible modifications to the fitting formulae that may minimize the error introduced by these extrapolations.

3.2 Circular velocity profiles

Many observations, such as disc galaxy rotation curves or strong gravitational lensing, are better probes of the *cumulative* mass distribution than of the differential density profile shown in Fig. 1. Since cumulative profiles are subject to different uncertainties from differential ones, it is important to verify that our conclusions regarding the suitability of the NFW or M99 fitting formulae are also applicable to the cumulative mass distribution of ΛCDM haloes.

The radial dependence of the spherically averaged circular velocity profile of all haloes in our series is shown in Fig. 2. As in Fig. 1, the thick solid curves in the top-left (right) panel are meant to illustrate a typical NFW (M99) profile corresponding to dwarf, galaxy and cluster haloes, respectively. The bottom-left and -right panels show deviations from the *best* fit to each halo using the NFW or M99 profile, respectively. Both profiles reproduce the cumulative mass profile of the simulated haloes reasonably well. The largest deviations seen are for the M99 fits, but they do not exceed 25 per cent over the radial range resolved in the simulations. NFW fits fare better, with deviations that do not exceed 10 per cent.

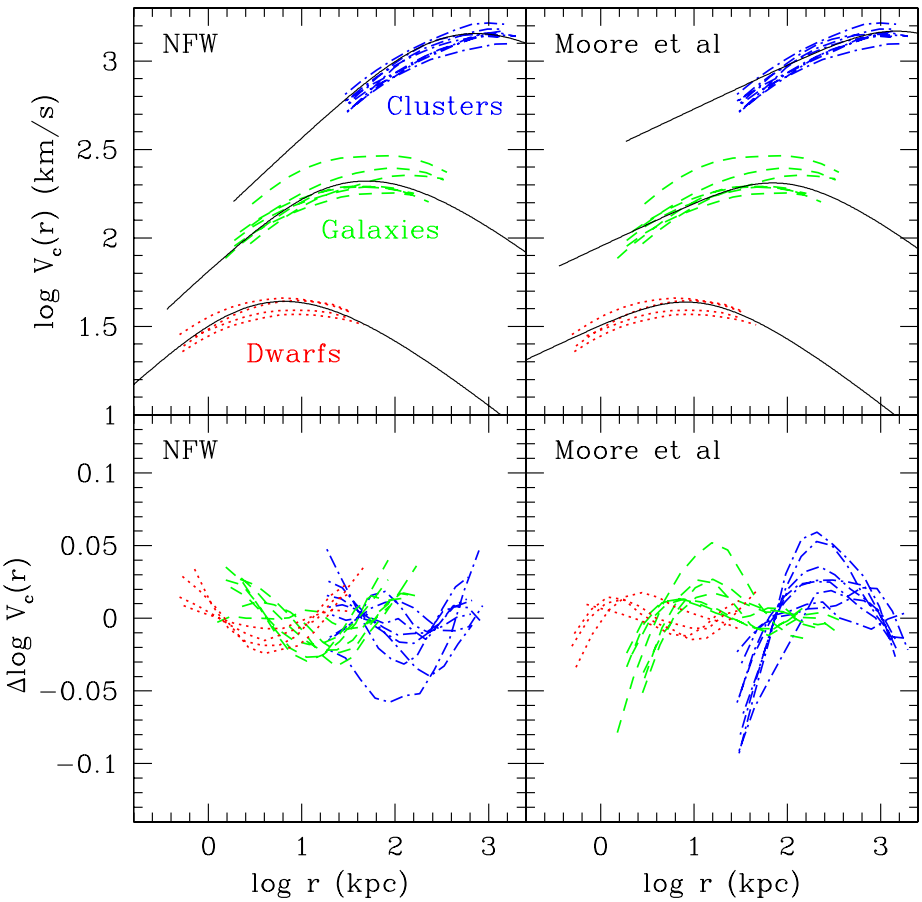

Figure 2. Spherically averaged circular velocity $[V_{\rm c}(r) = \sqrt{GM(r)/r}]$ profiles of all our simulated haloes. As in Fig. 1, circular velocities are computed in radial bins of equal logarithmic width and are shown from the innermost converged radius ($r_{\rm conv}$) out to about the virial radius (r_{200}) of each halo. Our simulations target haloes in three distinct mass groups: 'dwarf', 'galaxy' and 'cluster' haloes, spanning more than a factor of ∼50 in velocity. Thick solid lines in the top panels illustrate the expected profile for each mass range according to the fitting formula proposed by NFW (top left) or M99 (top right). The bottom panels indicate the deviation from the *best* fit achieved for each individual halo (simulation minus fit) with the NFW profile (equation 1) or with its modified form, as proposed by M99 (equation 2).

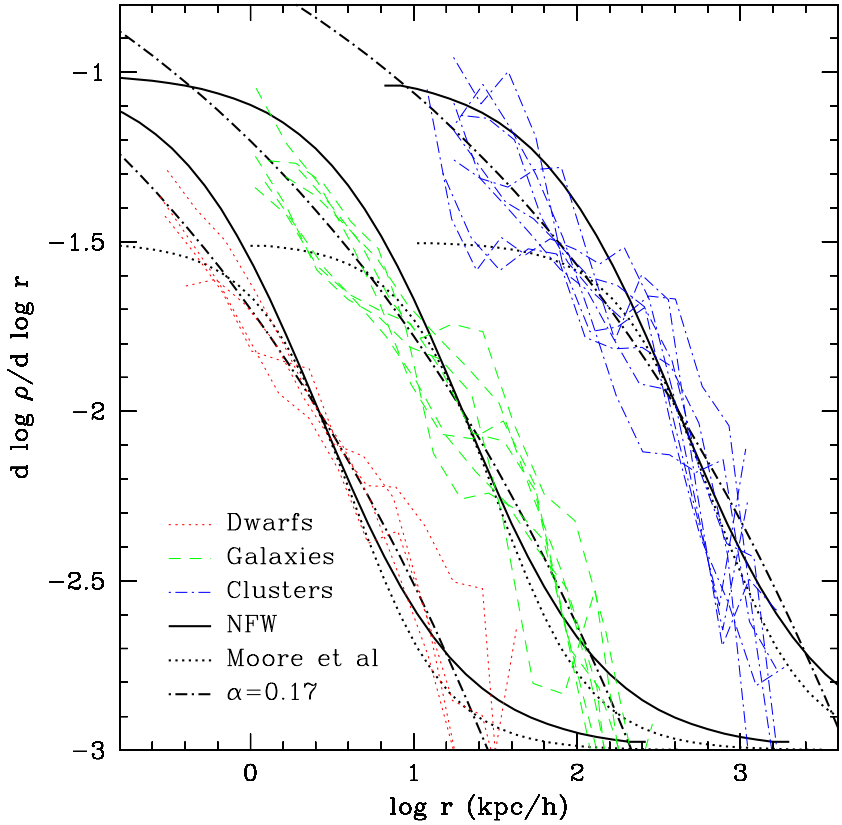

Figure 3. Logarithmic slope of the density profile of all haloes in our sample, plotted versus radius. Thick solid and dotted curves illustrate the radial dependence of the slope expected from the NFW profile (equation 1) and the modification proposed by M99 (equation 2), respectively. Note that although both fitting formulae have well-defined asymptotic inner slopes (−1 and −1.5, respectively) there is no sign of convergence to a well-defined value of the central slope in the simulated haloes. At the innermost converged radius, the simulated halo profiles are shallower than −1.5, in disagreement with the M99 profile. In addition, inside the radius at which the slope equals −2, r_{-2}, the profiles appear to get shallower more gradually than in the NFW formula. A power-law radial dependence of the slope seems to fit the results of our simulations better; the dot-dashed lines indicate the predictions of the ρ_α profile introduced in equations (4) and (5) for $\alpha = 0.17$. Best fits to individual haloes yield α values in the range 0.1–0.2 (see Table 3).

As with the density profiles, the deviations between simulation and fits, although small, increase toward the centre, suggesting that caution should be exercised when extrapolating these fitting formulae beyond the spatial region where they have been validated. This is important because observational data, such as disc galaxy rotation curves, often extend to regions inside the minimum convergence radius in these simulations.

3.3 Radial dependence of logarithmic slopes

We have noted in the previous subsections that systematic deviations are noticeable in both NFW and M99 fits to the mass profiles of simulated ΛCDM haloes. NFW fits tend to underestimate the dark matter density near the centre, whilst M99 fits tend to overestimate the circular velocity in the inner regions. The reason for this is that *neither* fitting formula fully captures the radial dependence of the density profile. We explore this in Fig. 3, which shows the logarithmic slope, $\mathrm{d}\ln\rho/\mathrm{d}\ln r \equiv -\beta(r)$, of all simulated haloes, as a function of radius. Although there is substantial scatter from halo to halo, a number of trends are robustly defined.

The first trend to note is that halo density profiles become shallower inward down to the innermost resolved radius, $r_{\rm conv}$ (the smallest radius plotted in Fig. 3). *We see no indication for convergence to a well-defined asymptotic value of the inner slope in our simulated haloes*, neither to the $\beta_0 = \beta(r = 0) = 1$ expected for the NFW profile (solid curves in Fig. 3) nor to the $\beta_0 = 1.5$ expected in the case of M99 (dotted curves in the same figure).

The second trend is that the radial dependence of the logarithmic slope deviates from what is expected from either the NFW or the M99 fitting formulae. Near $r_{\rm conv}$, the slopes are significantly shallower than $\beta_0 = 1.5$ (and thus in disagreement with the M99 formula) but they are also significantly steeper than expected from NFW fits. In quantitative terms, let us consider the slope well inside the characteristic radius, r_{-2} [where the slope takes the 'isothermal' value[2] of $\beta(r_{-2}) = 2$]. For cluster haloes, for example, at $r = 0.1r_{-2}$ ($\sim$50 h^{-1} kpc) the average slope is approximately −1.3, whereas the NFW formula predicts ~ -1.18 and M99 predicts ~ -1.5. This is in agreement with the latest results of Fukushige, Kawai & Makino (2003), who also report profiles shallower than $r^{-1.5}$ at the innermost converged radius of their simulations. A best-fitting slope of $r^{-1.3}$ was also reported by Moore et al. (2001) for a dwarf galaxy halo (of mass similar to the Draco dwarf spheroidal), although that

[2] The characteristic radius, r_{-2}, as well as the density at that radius, $\rho_{-2} \equiv \rho(r_{-2})$, can be measured directly from the simulations, without reference to or need for any particular fitting formula. For the NFW profile, r_{-2} is equivalent to the scale radius $r_{\rm s}$ (see equation 1). The density at r_{-2} is related to the NFW characteristic density, $\rho_{\rm s}$, by $\rho_{-2} \equiv \rho(r_{-2}) = \rho_{\rm s}/4$.

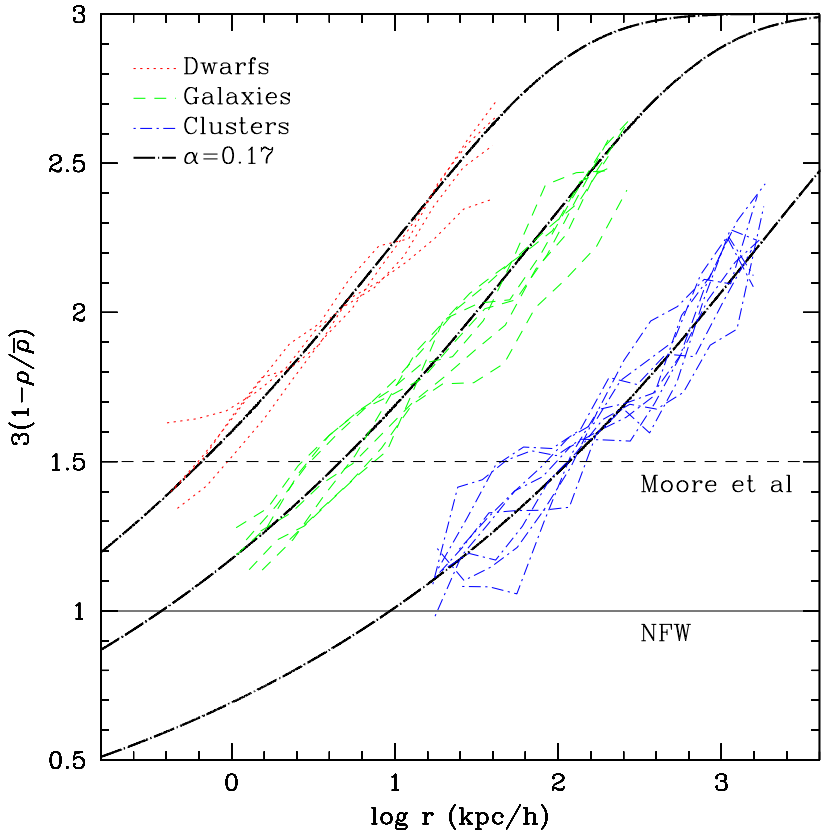

Figure 4. Maximum asymptotic inner slope compatible with the mean density interior to radius r, $\bar{\rho}(r)$, and with the local density at that radius, $\rho(r)$. This provides a robust limit to the central slope, $\beta_0 < \beta_{\rm max}(r) = -3[1 - \rho(r)/\bar{\rho}(r)]$, under the plausible assumption that β is monotonic with radius. Note that there is not enough mass within the innermost converged radius in our simulations to support density cusps as steep as $r^{-1.5}$. The asymptotic slope of the NFW profile, $\beta_0 = 1$, is still compatible with the simulated haloes, although there is no convincing evidence for convergence to a well-defined power-law behaviour in any of our simulated haloes. The thick dot-dashed curves illustrate the expected radial dependence of $\beta_{\rm max}$ for the ρ_α profile introduced in Section 3.6, for $\alpha = 0.17$.

simulation was stopped at $z = 4$, and might therefore not be directly comparable to the results we present here.

This discrepancy in the radial dependence of the logarithmic slope between simulations and fitting formulae is at the root of the different interpretations of the structure of the central density cusp proposed in the literature. For example, because profiles become shallower inward more gradually than in the NFW formula, modifications with more steeply divergent cusps (such as equation 2) tend to fit density profiles (but not circular velocity profiles) better in the region interior to r_{-2}. This is *not*, however, a sure indication of a steeper cusp. Indeed, *any* modification to the NFW profile that results in a more gradual change in the slope inside r_{-2} will lead to improved fits, *regardless* of the value of the asymptotic central slope. We show this explicitly in Section 3.6.

3.4 Maximum asymptotic slope

Conclusive proof that the central density cannot diverge as steeply as $\beta_0 = 1.5$ is provided by the total mass inside the innermost resolved radius, $r_{\rm conv}$. This is because, at any radius r, the mean density, $\bar{\rho}(r)$, together with the local density, $\rho(r)$, provides a robust upper limit to the asymptotic inner slope. This is given by $\beta_{\rm max}(r) = 3[1 - \rho(r)/\bar{\rho}(r)] > \beta_0$, under the plausible assumption that β is monotonic with radius.

Fig. 4 shows $\beta_{\rm max}$ as a function of radius; clearly, except for possibly one dwarf system, no simulated halo has enough dark mass within $r_{\rm conv}$ to support cusps as steep as $r^{-1.5}$. The NFW asymptotic slope, corresponding to $\beta_0 = 1$, is still consistent with the simulation data, but the actual central value of the slope may very well be shallower. We emphasize again that there is no indication for convergence to a well-defined value of β_0: density profiles become shallower inward down to the smallest resolved radius in the simulations.

3.5 A 'universal' density profile

Fig. 3 also shows that there is a well-defined trend with mass in the slope of the density profile measured at $r_{\rm conv} \sim 0.005$ to $0.01 r_{200}$ (the innermost point plotted for each profile): $\beta(r_{\rm conv}) \sim 1.1$ for clusters, $\sim$1.2 for galaxies and $\sim$1.35 for dwarfs. A similar trend was noted by Jing & Suto (2000), who used it to argue against a 'universal' density profile shape. However, as discussed by Klypin et al. (2001), this is just a reflection of the trend between the concentration of a halo and its mass. It does *not* indicate any departure from similarity in the profile shape. Indeed, one does *not* expect the profiles of haloes of widely different mass, such as those in our series, to have similar slopes at a constant fraction of the virial radius. Rather, if the density profiles are truly self-similar, slopes ought to coincide at fixed fractions of a *mass-independent* radial scale, such as r_{-2}.

Fig. 5(top) shows the striking similarity between the structures of haloes of different mass when all density profiles are scaled to r_{-2} and $\rho_{-2} \equiv \rho(r_{-2})$. The density profile of a dwarf galaxy halo then

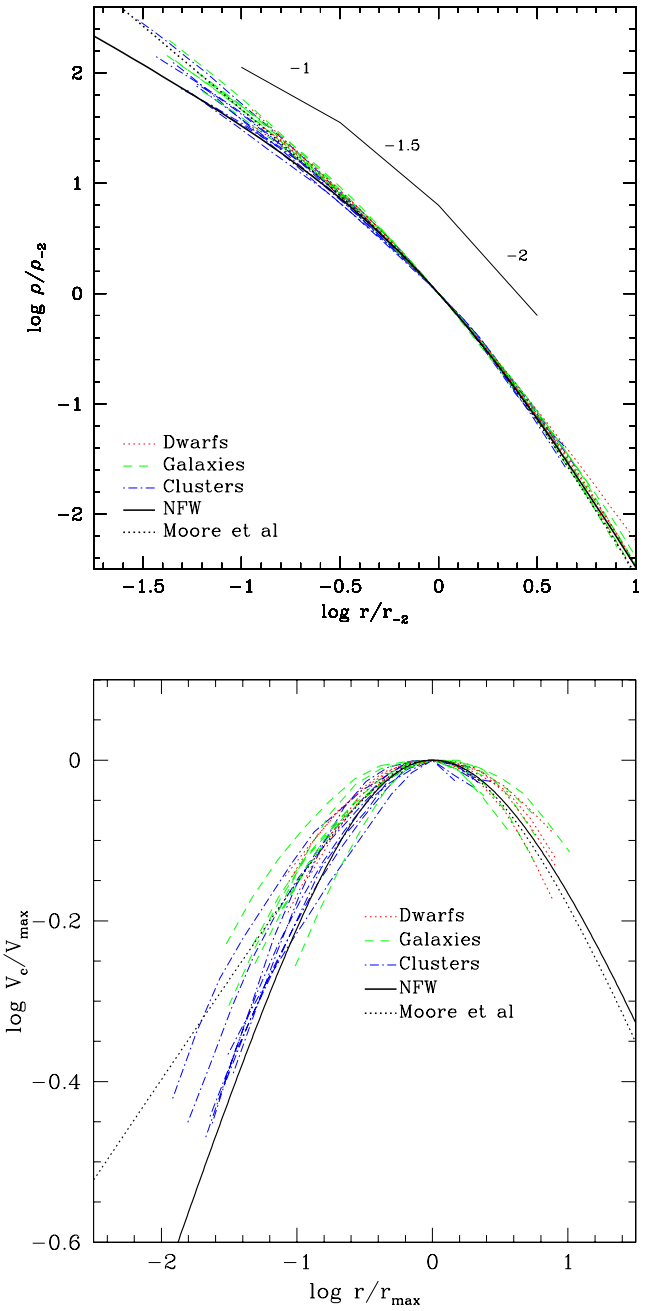

Figure 5. (Top) Density profiles of all haloes in our series, scaled to the radius, r_{-2}, where the local logarithmic slope of the density profile takes the isothermal value of $\beta = -\,\mathrm{d}\log\rho/\mathrm{d}\log r = 2$. Densities are scaled to $\rho_{-2} = \rho(r_{-2})$. This figure shows that, with proper scaling, there is little difference in the shape of the density profile of haloes of different mass, confirming the 'universal' nature of the mass profile of ΛCDM haloes. The NFW profile (equation 1) is a fixed curve in these scaled units, and is shown with a thick solid line. The M99 formula (equation 2) is shown with a dashed line. (bottom) Circular velocity profiles of all haloes in our series, scaled to the maximum velocity, $V_{\rm max}$, and to the radius at which it is reached, $r_{\rm max}$. Note the significant scatter from halo to halo, and also that the NFW and M99 profiles appear to bracket the extremes of the mass profile shapes of haloes in our simulation series.

differs very little from that of a galaxy cluster 10^5 times more massive. This demonstrates that spherically averaged density profiles are approximately 'universal' in shape; rarely do individual density profiles deviate from the scaled average by more than ∼50 per cent.

In the scaled units of Fig. 5, the NFW and M99 profiles are fixed, and are shown as solid and dotted curves, respectively. With this scaling, differences between density profiles are more evident than when best fits are compared, since the latter – by definition – minimize the deviations. In Fig. 5(top), for example, it is easier to recognize the 'excess' of dark mass inside r_{-2} relative to the NFW profile that authors such as M99 and Fukushige & Makino (1997, 2001, 2003) have (erroneously) interpreted as implying a steeply divergent density cusp.

The similarity in mass profile shapes is also clear in Fig. 5(bottom), which shows the circular velocity curves of all haloes in our series, scaled to the maximum, $V_{\rm max}$, and to the radius where it is reached, $r_{\rm max}$. NFW and M99 are again fixed curves in these scaled units. This comparison is more relevant to observational interpretation, since rotation curve, stellar dynamical and lensing tracers are all more directly related to $V_{\rm c}(r)$ than to $\rho(r)$. Owing to the reduced dynamic range of the y-axis, the scatter in mass profiles from halo to halo is more clearly apparent in the $V_{\rm c}$ profiles; the NFW and M99 profiles appear approximately to bracket the extremes in the mass profile shapes of simulated haloes. We discuss below a simple fitting formula that, with the aid of an extra parameter, is able to account for the variety of mass profile shapes better than either the NFW or M99 formulae.

3.6 An improved fitting formula

Although the discussion in the previous subsections has concentrated on global deviations from simple fitting formulae such as NFW or M99, it is important to re-emphasize that such deviations, although significant, are actually rather small. As shown in Fig. 2, NFW best fits reproduce the circular velocity profiles to an accuracy of better than ∼10 per cent down to roughly 0.5 per cent of r_{200}. Although this level of accuracy may suffice for some observational applications, the fact that deviations increase inward and are maximal at the innermost converged point suggests the desirability of a new fitting formula better suited for extrapolation to regions beyond those probed reliably by simulations.

An improved fitting formula ought to reproduce: (i) the more gradual shallowing of the density profile towards the centre; (ii) the apparent lack of evidence for convergence to a well-defined central power law; and (iii) the significant scatter in profile shape from halo to halo. After some experimentation, we have found that a density profile where $\beta(r)$ is a power law of radius is a reasonable compromise that satisfies these constraints whilst retaining simplicity, i.e.

$$\beta_\alpha(r) = -\mathrm{d}\ln\rho/\mathrm{d}\ln r = 2(r/r_{-2})^\alpha, \qquad (4)$$

which corresponds to a density profile of the form

$$\ln(\rho_\alpha/\rho_{-2}) = (-2/\alpha)[(r/r_{-2})^\alpha - 1]. \qquad (5)$$

This profile has finite total mass (the density cuts off exponentially at large radius) and has a logarithmic slope that decreases inward more gradually than the NFW or M99 profiles. The thick dot-dashed curves in Figs 3 and 4 show that equation (5) (with $\alpha \sim 0.17$) does indeed reproduce fairly well the radial dependence of $\beta(r)$ and $\beta_{\rm max}(r)$ in simulated haloes.

Furthermore, adjusting the parameter α allows the profile to be tailored to each individual halo, resulting in improved fits. Indeed, as shown in Fig. 6, equation (5) reproduces the density profile of individual haloes to better than ∼10 per cent over the reliably resolved radial range, and there is no discernible radial trend in the residuals. This is a significant improvement over NFW or M99 fits, where the

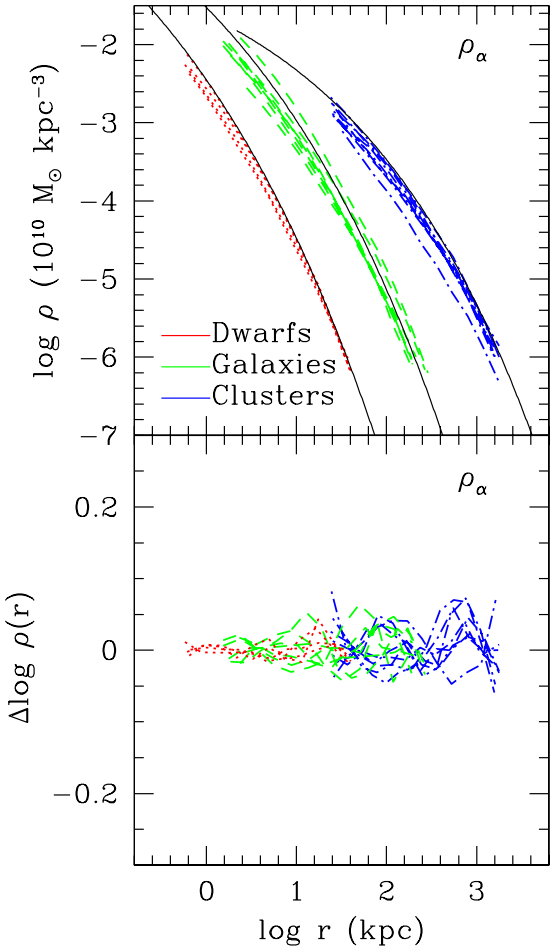

Figure 6. As Fig. 1, but for the ρ_α fitting formula presented in equation (5). The thick solid lines in the top panels illustrate the expected halo profile for each mass range according to the prescription proposed by NFW. The bottom panels indicate the deviation from the ρ_α *best* fit achieved for each individual halo, taking α as a free parameter. Note the improvement in the fits compared with those achieved with the NFW or M99 profiles and shown in Fig. 1.

maximum deviations were found at the innermost resolved radius. The best-fitting values of α (in the range 0.1–0.2) show no obvious dependence on halo mass, and are listed in Table 3. The average α value is 0.172 and the dispersion about the mean is 0.032.

We note that the ρ_α profile is not formally divergent, and converges to a finite density at the centre, $\rho_0 = e^{2/\alpha}\rho_{-2} \sim 6 \times 10^5\ \rho_{-2}$ (for $\alpha = 0.15$). It is unclear at this point whether such asymptotic behaviour is a true property of ΛCDM haloes or simply an artefact of the fitting formula that results from choosing $\beta_0 = 0$ in equation (4). The simulations show no evidence for convergence to a well-defined central value for the density, but even in the best-resolved cases they only probe regions where densities do not exceed $\sim 10^2\ \rho_{-2}$. This is, for α in the range 0.1–0.2, several orders of magnitude below the maximum theoretical limit in equation (5).

We also note that the convergence to $\beta_0 = 0$ is quite slow for the values of α favoured by our fits. Indeed, for $\alpha = 0.1$, the logarithmic slope only reaches a value significantly shallower than the NFW asymptotic slope at radii that are well inside the convergence radius of our simulations; for example, $\beta_\alpha(r)$ only reaches 0.5 at $r = 9.5 \times 10^{-7} r_{-2}$, corresponding to $r \sim 0.01$ pc for galaxy-sized haloes. This implies that the ρ_α profile is in practice 'cuspy' for most astrophysical applications. Establishing conclusively whether ΛCDM haloes actually have divergent inner density cusps is a task that awaits simulations with much improved resolution than those presented here.

3.7 Comparisons between fitting formulae

Fig. 7 compares the density and circular velocity profiles implied by the ρ_α formula (equation 5) with the NFW and M99 profiles (left panels), as well as with the fitting formula proposed by Stoehr et al. (2002, hereafter SWTS) to describe the structure of *substructure* haloes (right panels).

The top-left panel of Fig. 7 shows that, despite its finite central density, the ρ_α profile can approximate fairly well both an NFW profile (for $\alpha \sim 0.2$) and an M99 profile (for $\alpha \sim 0.1$) for over three decades in radius. The circular velocity profile for $\alpha = 0.2$ is likewise quite similar to that of NFW (bottom-left panel of Fig. 7), but the similarity to the shape of the M99 V_c profile is less for all values of α.

Interestingly, the V_c profiles corresponding to ρ_α resemble parabolae in a log–log plot, and thus may also be used to approximate the mass profiles of substructure haloes, as discussed by SWTS. This is demonstrated in the bottom-right panel of Fig. 7, where we show that the V_c profiles corresponding to $\alpha = 0.1$, 0.2 and 0.7, are very well approximated by the SWTS formula, i.e.

$$\log(V_c/V_{max}) = -a[\log(r/r_{max})]^2, \qquad (6)$$

for $a = 0.09$, 0.17 and 0.45, respectively. The latter value ($a = 0.45$ or $\alpha = 0.7$) corresponds to the median of the SWTS best fits to the mass profile of substructure haloes. Note that this is quite different from the α value of ~ 0.1–0.2 required to fit isolated ΛCDM haloes (see Table 3).

It might actually be preferable to adopt the ρ_α profile rather than the SWTS formula for describing substructure haloes, since $\rho_\alpha(r)$ is monotonic with radius and extends over all space. This is not the case for SWTS, as shown in the top-right panel of Fig. 7. The SWTS density profiles are 'hollow' (i.e. the density has a minimum at the centre), and extend out to a maximum radius, given by $e^{1/4a} r_{max}$. This is because the circular velocity in the outer regions of the SWTS formula falls off faster than Keplerian, and therefore the corresponding density becomes formally negative at a finite radius.

The ρ_α profile thus appears versatile enough to reproduce, with a single fitting parameter, the structure of ΛCDM haloes and their substructures. As ρ_α captures the inner slopes better than either the NFW or M99 profiles, it is also likely to be a safer choice should extrapolation of the mass profile beyond the converged radius prove necessary. We end by emphasizing, however, that all simple fitting formulae have shortcomings, and that *direct comparison with simulations rather than with fitting formulae should be attempted whenever possible*.

3.8 Scaling parameters

The application of fitting formulae such as the one described above requires a procedure for calculating the characteristic scaling parameters for a given halo mass, once the power spectrum and cosmological parameters are specified. NFW developed a simple procedure for calculating the parameters corresponding to haloes of a given mass. Owing to the close relationship between the scale radius, r_s, and characteristic density, ρ_s, of the NFW profile and the r_{-2} and ρ_{-2} parameters of equation (5), we can use the formalism developed by NFW to compute the expected values of these parameters in a given cosmological model.

Table 3. The fit and structural parameters of the resimulated haloes.

Label	r_{-2} (h^{-1} kpc)	ρ_{-2} ($\rho_{\rm crit}$)	$r_{\rm max}$ (h^{-1} kpc)	$V_{\rm max}$ (km s^{-1})	$r_{\rm s}$ (h^{-1} kpc)	$\rho_{\rm s}$ ($\rho_{\rm crit}$)	$r_{\rm M}$ (h^{-1} kpc)	$\rho_{\rm M}$ ($\rho_{\rm crit}$)	α
D1	3.23	1.12 e4	6.07	39.1	2.59	7.03 e4	5.38	7.58 e3	0.164
D2	3.04	1.58 e4	6.64	44.2	2.43	9.61 e4	2.27	1.17 e5	0.211
D3	2.57	1.58 e4	6.35	36.9	2.94	5.01 e4	4.05	2.51 e4	0.122
D4	2.57	2.24 e4	4.27	45.7	2.06	1.49 e5	2.18	1.36 e5	0.166
G1	18.5	6.76 e3	23.7	1.95 e2	23.2	4.06 e4	19.4	8.43 e4	0.142
G2	28.0	2.40 e3	68.5	1.78 e2	16.8	1.13 e5	19.4	8.43 e4	0.191
G3	20.2	6.31 e3	43.4	1.96 e2	28.0	1.52 e4	47.3	8.24 e3	0.142
G4	29.6	4.37 e3	63.4	2.49 e2	12.3	6.78 e4	16.8	3.44 e4	0.177
G5	20.7	1.58 e4	67.7	2.91 e2	13.8	5.20 e4	15.3	4.23 e4	0.184
G6	39.6	2.00 e3	96.4	2.26 e2	15.3	3.79 e4	20.7	2.03 e4	0.171
G7	16.4	1.26 e4	29.9	1.94 e2	13.4	6.22 e4	14.9	5.15 e4	0.138
C1	5.84 e2	4.68 e2	1.03 e3	1.48 e3	440	3.36 e3	661	1.58 e3	0.133
C2	3.95 e2	1.15 e3	9.99 e2	1.51 e3	362	5.17 e3	396	4.46 e3	0.215
C3	3.27 e2	1.12 e3	6.15 e2	1.38 e3	249	9.07 e3	278	7.44 e3	0.188
C4	4.16 e2	7.94 e2	6.57 e2	1.38 e3	315	5.47 e3	339	4.91 e3	0.161
C5	2.87 e2	1.91 e3	6.48 e2	1.42 e3	271	8.45 e3	326	5.88 e3	0.215
C6	3.82 e2	1.32 e3	6.94 e2	1.64 e3	297	8.70 e3	302	8.75 e3	0.203
C7	5.69 e2	3.55 e2	1.25 e3	1.25 e3	283	3.92 e3	475	2.11 e3	0.129
C8	3.68 e2	1.00 e3	9.35 e2	1.44 e3	361	4.41 e3	345	5.04 e3	0.219

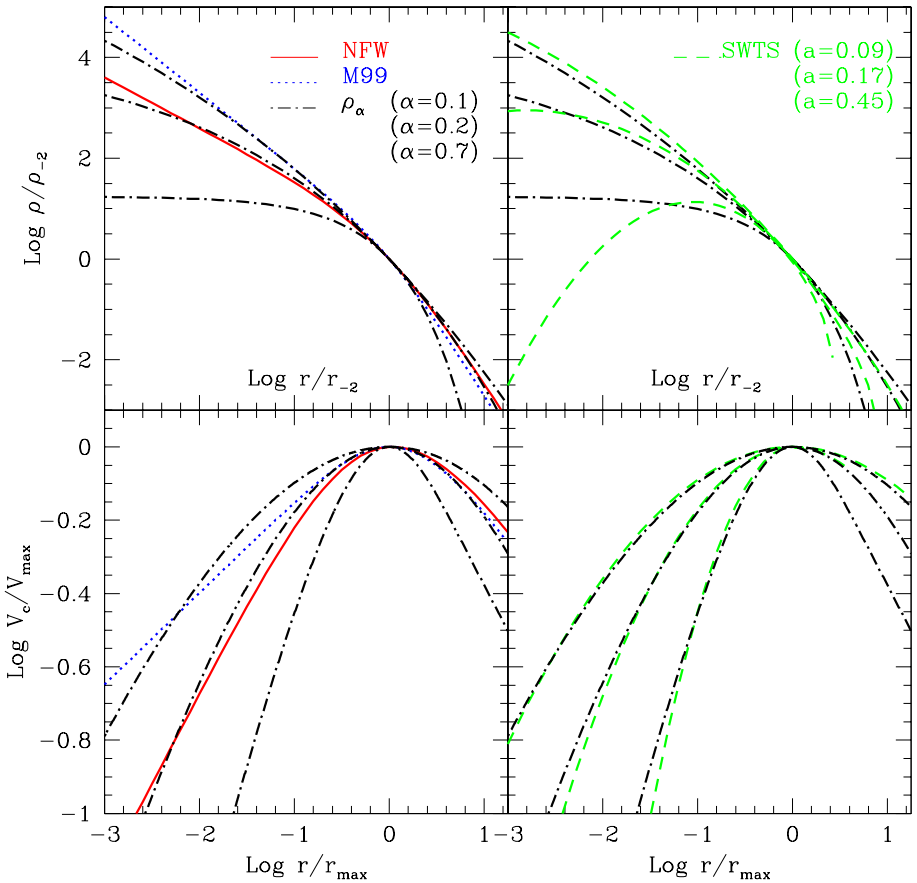

Figure 7. Comparison between the density (top) and circular velocity (bottom) profiles corresponding to four different fitting formulae: NFW (solid curves, equation 1), M99 (dotted curves, equation 2), SWTS (dashed curves, equation 6) and ρ_α (dot-dashed curves, equation 5). Circular velocity profiles are scaled to the maximum, $V_{\rm max}$, and to the radius where that is reached, $r_{\rm max}$. Density profiles are scaled as in Fig. 5. Note that, despite having a finite central density, the ρ_α formula matches, for about three decades in radius, the NFW profile (for $\alpha = 0.2$) or the M99 profile (for $\alpha = 0.1$, see top-left panel). It also matches closely the SWTS 'parabolic' circular velocity profiles intended to reproduce *substructure* haloes (see bottom-right panel); the $V_{\rm c}$ profile with $\alpha = 0.7$ is very similar to the SWTS profile with $a = 0.45$, the median value of the fits to substructure haloes reported by SWTS. See text for further discussion.

NFW interpreted the characteristic density of a halo as reflecting the density of the universe at a suitably defined time of collapse. Their formalism assigns to each halo of mass M (identified at $z = 0$) a collapse redshift, $z_{\rm coll}(M,\, f)$ defined as the epoch when half the mass of the halo was first contained in progenitors more massive than a certain fraction f of the final mass. With this definition, and once f has been chosen, $z_{\rm coll}$ can be computed using the Press–Schechter theory (e.g. Lacey & Cole 1993). The NFW model then assumes that the characteristic density of a halo (i.e. $\rho_{\rm s}$ in equation 1) is proportional to the mean density of the universe at $z_{\rm coll}$.

The redshift dependence of the characteristic density was first probed in detail by Bullock et al. (2001, hereafter B01), who proposed a modification to the model of NFW in which, for a given halo mass, the scale radius, $r_{\rm s}$, remains approximately constant with redshift. Eke et al. (2001, hereafter ENS), alternatively, argued that the characteristic density of a halo is determined by the *amplitude and shape* of the power spectrum, as well as by the universal expansion history. Their formalism reproduces nicely the original results of NFW as well as the redshift dependence pointed out by B01, and is applicable to more general forms of the power spectrum, including the 'truncated' power spectra expected in scenarios such as warm dark matter (see ENS for more details).

We have used the ENS and B01 formalisms to predict the halo mass dependence of the scaling parameters, ρ_{-2} and r_{-2}, and we compare the results with our simulations in Fig. 8. The ENS prediction is shown by the solid line whereas the dotted line shows that of B01. Both formalisms reproduce reasonably well the trend seen in the simulations, so that one can use either, in conjunction with equation (5) (with α in the range 0.1–0.2), to predict the structure of a ΛCDM halo. A simple code that computes r_{-2} and ρ_{-2} as a function of mass in various cosmological models is available upon request from the authors. Existing codes that compute NFW halo parameters as a function of mass and of other cosmological parameters may also be used, noting that $\rho_{-2} = \rho_{\rm s}/4$ and that $r_{-2} = r_{\rm s}$.

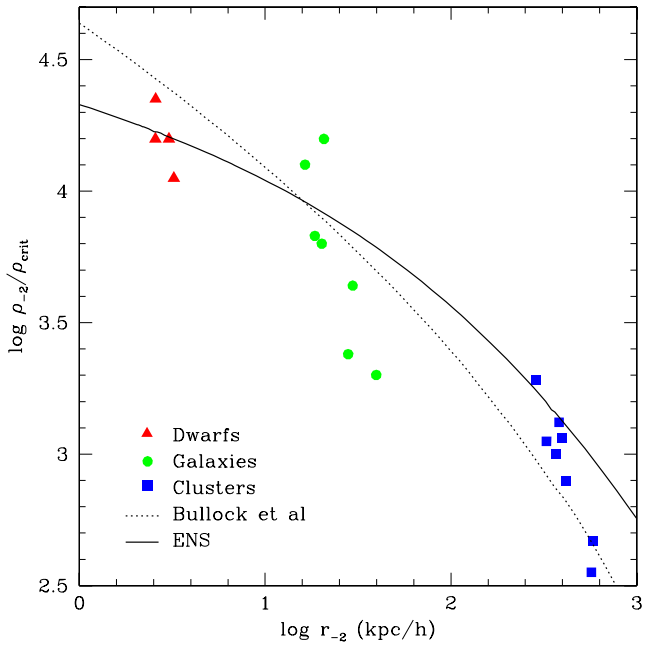

Figure 8. The radius, r_{-2}, where the logarithmic slope of the density profile takes the 'isothermal' value, $\beta(r_{-2}) = 2$, plotted versus the local density at that radius, $\rho_{-2} = \rho(r_{-2})$, for all simulated haloes in our series. This figure illustrates the mass dependence of the central concentration of dark matter haloes: low-mass haloes are systematically denser than their more massive counterparts. Solid and dotted lines indicate the scale radius-characteristic density correlation predicted by the formalisms presented by Eke et al. (2001) and Bullock et al. (2001). These parameters may be used, in conjunction with equation (5), to predict the mass profile of ΛCDM haloes.

Finally, we note that neither formalism captures perfectly the mass dependence of the characteristic density; small but significant deviations, as well as a sizable scatter, are evident in Fig. 8. Dwarf galaxy haloes appear to be less concentrated than predicted by the formalism proposed by B01; a similar observation applies to cluster haloes when compared with the predictions of ENS. Such shortcomings should be considered when deriving cosmological constraints from fits to observational data (see e.g. Zentner & Bullock 2002; McGaugh, Barker & de Blok 2003); and suggest again that direct comparison between observations and simulations is preferable to the use of fitting formulae.

4 SUMMARY

We have analysed the mass profile of ΛCDM haloes in a series of simulations of high mass, spatial and temporal resolution. Our series targets haloes spanning five decades in mass: 'dwarf' galaxy haloes with virial circular velocities of order $V_{200} \sim 30$ km s^{-1}; 'galaxy'-sized haloes with $V_{200} \sim 200$ km s^{-1}; and 'cluster' haloes with $V_{200} \sim 1200$ km s^{-1}. Each of the 19 haloes in our series was simulated with comparable numerical resolution: they have between 8×10^5 and 4×10^6 million particles within the virial radius, and have been simulated following the 'optimal' prescription for time-stepping and gravitational softening laid down in the numerical convergence study of P03.

The high resolution of our simulations allows us to probe the inner properties of the mass profiles of ΛCDM haloes, down to ∼0.5 per cent of r_{200} in our best resolved runs. These results have important implications for the structure of the inner cusp in the density profile and resolve some of the disagreements arising from earlier simulation work. Our main conclusions may be summarized as follows.

(i) ΛCDM halo density profiles are 'universal' in shape: i.e. a simple fitting formula reproduces the structure of all simulated haloes, regardless of mass. Both the NFW and the M99 profiles describe the density and circular velocity profiles of simulated haloes reasonably well. NFW best fits to the circular velocity profiles deviate by <10 per cent over the region that is well resolved numerically. M99 best fits reproduce circular velocity profiles to better than 25 per cent over the same region. It should be noted, however, that the deviations increase inwards and are typically maximal at the innermost resolved radius, a result that warns against extrapolating to smaller radii with these fitting formulae.

(ii) ΛCDM haloes appear to be 'cuspy': i.e., the dark matter density increases monotonically towards the centre with no evidence for a well-defined 'core' of constant density. We find no evidence, however, for a central asymptotic power-law bin the density profiles. These become progressively shallow inwards and are significantly shallower than isothermal at the innermost resolved radius, $r_{\rm conv}$. At $r \sim 0.01\, r_{200}$, the average slopes of 'cluster', 'galaxy' and 'dwarf' haloes are $\beta(r_{\rm conv}) \sim 1.1$, ∼1.2 and ∼1.35, respectively. This is steeper than predicted by the NFW profile but shallower than the asymptotic slope of the M99 profile.

(iii) The density and enclosed mass at $r_{\rm conv}$ may be used to derive an upper limit on any asymptotic value of the inner slope. Cusps as steep as $\beta_0 = 1.5$ are confidently ruled out in essentially all cases; the

asymptotic slope of the NFW profile ($\beta_0 = 1$) is still consistent with our data. The radial dependence of $\beta(r)$ differs from that of the NFW profile, however, decreasing more slowly with decreasing radius than is predicted. For some scalings of the NFW fitting formula to the numerical data, this shape difference appears as a dark matter 'excess' near the centre which has (erroneously) been interpreted indicating a steeply divergent density cusp.

(iv) A simple formula where $\beta(r)$ is a power law of radius reproduces the gradual radial variation of the logarithmic slope and its apparent failure to converge to any specific asymptotic value (equation 5). This formula leads to much improved fits to the density profiles of simulated haloes, and may prove a safer choice when comparison with observational data demands extrapolation below the innermost converged radii of the simulations.

Our study demonstrates that, although simple fitting formulae such as those found in NFW are quite accurate in describing the global structure of ΛCDM haloes, one should be aware of the limitations of these formulae when interpreting observational constraints. Extrapolation beyond the radial range where these formulae have been validated is likely to produce substantial errors. Proper account of the substantial scatter in halo properties at a given halo mass also appears necessary when assessing the consistency of observations with a particular cosmological model. Direct comparison between observations and simulations (rather than with fitting formulae) is clearly preferable whenever possible. Given the computational challenge involved in providing consistent, robust and reproducible theoretical predictions for the inner structure of CDM haloes, it is likely that observational constraints will exercise to the limit our hardware and software capabilities for some time to come.

ACKNOWLEDGMENTS

This work has been supported by computing time generously provided by the High Performance Computing Facility at the University of Victoria, as well as by the Edinburgh Parallel Computing Centre and by the Institute for Computational Cosmology at the University of Durham. Expert assistance by Colin Leavett-Brown in Victoria and Lydia Heck in Durham is gratefully acknowledged. JFN is supported by the Alexander von Humboldt Foundation, the Natural Sciences and Engineering Research Council of Canada, and the Canadian Foundation for Innovation.

REFERENCES

Bardeen J. M., Bond J. R., Kaiser N., Szalay A. S., 1986, ApJ, 304, 15
Binney J., 2004, MNRAS, in press (astro-ph/0311155)
Bullock J. S., Kolatt T. S., Sigad Y., Somerville R. S., Kravtsov A. V., Klypin A. A., Primack J. R., Dekel A., 2001, MNRAS, 321, 559 (B01)
Calcáneo-Roldán C., Moore B., 2000, Phys. Rev. D, 62, 123005
Cole S., Lacey C., 1996, MNRAS, 281, 716
Crone M. M., Evrard A. E., Richstone D. O., 1994, ApJ, 434, 402
Davis M., Efstathiou G., Frenk C. S., White S. D. M., 1985, ApJ, 292, 371
Debattista V. P., Sellwood J. A., 1998, ApJ, 493, L5
Dubinski J., Carlberg R. G., 1991, ApJ, 378, 496
Eke V. R., Navarro J. F., Steinmetz M., 2001, ApJ, 554, 114 (ENS)
Flores R. A., Primack J. R., 1994, ApJ, 427, L1
Frenk C. S., White S. D. M., Davis M., Efstathiou G., 1988, ApJ, 327, 507
Fukushige T., Makino J., 1997, ApJ, 477, L9
Fukushige T., Makino J., 2001, ApJ, 557, 533
Fukushige T., Makino J., 2003, ApJ, 588, 674
Fukushige T., Kawai A., Makino J., 2003, ApJ, submitted (astro-ph/0306203)
Ghigna S., Moore B., Governato F., Lake G., Quinn T., Stadel J., 2000, ApJ, 544, 616
Hayashi E. et al., 2004, MNRAS, submitted (astro-ph/0310576)
Huss A., Jain B., Steinmetz M., 1999, ApJ, 517, 64
Jing Y. P., Suto Y., 2000, ApJ, 529, L69
Klypin A., Kravtsov A. V., Bullock J. S., Primack J. R., 2001, ApJ, 554, 903
Lacey C., Cole S., 1993, MNRAS, 262, 627
McGaugh S. S., de Blok W. J. G., 1998, ApJ, 499, 41
McGaugh S. S., Barker M. K., de Blok W. J. G., 2003, ApJ, 584, 566
Moore B., 1994, Nat, 370, 629
Moore B., Quinn T., Governato F., Stadel J., Lake G., 1999, MNRAS, 310, 1147 (M99)
Moore B., Calcáneo-Roldán C., Stadel J., Quinn T., Lake G., Ghigna S., Governato F., 2001, Phys. Rev. D, 64, 63508
Navarro J. F., Frenk C. S., White S. D. M., 1996, ApJ, 462, 563
Navarro J. F., Frenk C. S., White S. D. M., 1997, ApJ, 490, 493 (NFW)
Power C., Navarro J. F., Jenkins A., Frenk C. S., White S. D. M., Springel V., Stadel J., Quinn T., 2003, MNRAS, 338, 14 (P03)
Ricotti M., 2003, MNRAS, 344, 1237
Seljak U., Zaldarriaga M., 1996, ApJ, 469, 437
Springel V., Yoshida N., White S. D. M., 2001, New Astron., 6, 79
Stadel J., 2001, PhD thesis, University of Washington
Stoehr F., White S. D. M., Tormen G., Springel V., 2002, MNRAS, 335, L84 (SWTS)
Subramanian K., Cen R., Ostriker J. P., 2000, ApJ, 538, 528
Taylor J. E., Navarro J. F., 2001, ApJ, 563, 483
Taylor J. E., Silk J., 2003, MNRAS, 339, 505
van den Bosch F. C., Robertson B. E., Dalcanton J. J., de Blok W. J. G., 2000, AJ, 119, 1579
Yoshida N., Sheth R. K., Diaferio A., 2001, MNRAS, 328, 669
Zentner A. R., Bullock J. S., 2002, Phys. Rev. D, 66, 43003

This paper has been typeset from a TEX/LATEX file prepared by the author.